

# Multi-wavelength Calibration Procedure for the Pierre Auger Observatory Fluorescence Detectors

A.C. Rovero<sup>\*,a,1</sup>, P. Bauleo<sup>b</sup>, J.T. Brack<sup>b</sup>, J.L. Harton<sup>b</sup>, and R. Knapik<sup>b</sup>, for the Pierre Auger Collaboration

<sup>a</sup>*Instituto de Astronomía y Física del Espacio (CONICET), CC 67 Suc 28 (C1428ZAA) Buenos Aires, Argentina*

<sup>b</sup>*Colorado State University, Department of Physics, Fort Collins CO 80523, USA*

---

## Abstract

We present a method to measure the relative spectral response of the Pierre Auger Observatory Fluorescence Detector. The calibration was done at wavelengths of 320, 337, 355, 380 and 405 nm using an end-to-end technique in which the response of all detector components are combined in a single measurement. A xenon flasher and notch-filters were used as the light source for the calibration device. The overall uncertainty is 5%.

*Key words:* Auger Observatory, Extensive Air Shower, Fluorescence detectors, calibration, cosmic ray

*PACS:* 95.55.Cs, 96.50.sd

---

---

\*Corresponding author. e-mail: rovero@iafe.uba.ar

<sup>1</sup>Member of Carrera del Investigador, CONICET

## 1 1. Introduction

2 The Pierre Auger Observatory has been designed to measure Extensive  
3 Air Showers (EAS) initiated by cosmic rays with energies above  $10^{18}$  eV.  
4 The Observatory calls for the construction of two large detectors, one in the  
5 southern hemisphere and one in the northern hemisphere, each covering an  
6 area of at least  $3000 \text{ km}^2$  [1]. The Southern Observatory original baseline  
7 design in Malargüe, Argentina, is completed and consists of two detectors,  
8 the Surface Detector (SD) and the Fluorescence Detector (FD). The SD is  
9 composed of 1600 water Cherenkov detectors located on a triangular array  
10 of 1.5 km spacing to measure the EAS secondary particles reaching ground  
11 level. In addition, the UV-nitrogen fluorescence light produced in air is reg-  
12 istered by the FD during dark, clear nights. The FD consists of 24 telescopes  
13 distributed in four buildings, or FD stations, overlooking the SD array.

14 The energy calibration of data taken at the Pierre Auger Observatory  
15 relies on the calibration of the FD [2] [3]. A detailed description of the  
16 fluorescence detector can be found elsewhere [4]. The Auger FD telescopes  
17 use Schmidt optics. The aperture is defined by a 2.2 m optical diaphragm.  
18 A UV filter covers the aperture and reduces background light by cutting out  
19 all light not in the main part of the nitrogen fluorescence spectrum ( $\sim 300$   
20 - 400 nm). It also provides ambient isolation, which allows for temperature  
21 controlled operation of the telescope and prevents dust from entering the  
22 optical system. Spherical aberrations are reduced by a Schmidt corrector  
23 annulus covering only the outer portion of the aperture. Light is concentrated  
24 by a  $3.5 \text{ m} \times 3.5 \text{ m}$  tessellated spherical mirror into an array of 440 hexagonal  
25 photomultipliers (PMTs), referred to as “pixels”, with a field of view of 1.5  
26 deg each. At the focal plane, light concentrators approximating hexagonal  
27 Winston cones reduce dead spaces between PMTs. The pixel array is referred  
28 to as a “camera”. In Fig. 1 we show the main components of the FD telescope.

29 To calibrate the FD three different procedures are performed [5]: the rel-  
30 ative, the absolute and the multi-wavelength calibrations. Relative calibra-  
31 tion is performed at least at the beginning and at the end of every observing  
32 night. It is based on uncalibrated but stable light sources that illuminate  
33 the camera from three positions upstream in the optical system, tracking the  
34 nightly response variations of the whole system [6]. The absolute calibration  
35 is made by an end-to-end technique, using a calibrated portable light source  
36 in front of the telescope aperture, which calibrates the combined effect of  
37 each component in a single measurement at a single wavelength, 375 nm.

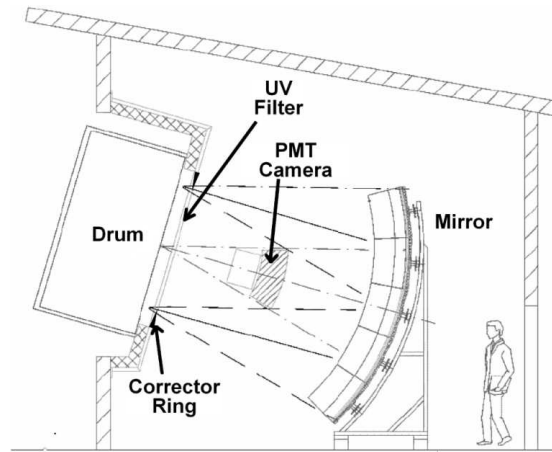


Figure 1: Sketch of the fluorescence detector showing its main components, together with the calibration light source (drum) in calibration position. PMT camera supports and drum supports are not shown for clarity.

38 The light source has been designed to uniformly illuminate all 440 pixels in  
 39 a single camera simultaneously and is referred to as the “drum” because of  
 40 its appearance. It is a cylinder of 2.5 m diameter and 1.4 m deep, with one  
 41 Teflon<sup>®</sup> face, and internally laminated with Tyvek<sup>®</sup> (see Fig. 2). When  
 42 used for absolute calibration of FD telescopes, a UV LED is placed inside  
 43 a small Teflon diffuser inside the drum, and surrounded by other diffusive  
 44 pieces in such a way that the face is uniformly illuminated. The procedure  
 45 to calibrate the drum at the laboratory has been outlined elsewhere for the  
 46 prototype [7] and for the current version of the drum [8]. Absolute calibra-  
 47 tion of FD telescopes is performed typically twice a year to follow long term  
 48 variations of the system response. Finally, a “multi-wavelength calibration”  
 49 procedure determines the spectral response of the system as a function of  
 50 photon wavelength. This is a relative measurement, normalised to the abso-  
 51 lute calibration at 375 nm. The multi-wavelength calibration is needed not  
 52 only for correct event reconstruction but also to correlate with the results  
 53 of alternative absolute calibrations performed at different wavelengths using  
 54 lasers. Changes in the spectral response of the FD are not expected to oc-  
 55 cur in the short term, thus the frequency for evaluating this dependence is  
 56 planned to be less than once per year.

57 In this work, we describe the procedure for multi-wavelength calibration of

58 fluorescence telescopes using an end-to-end technique similar to that used for  
59 the absolute calibration. We describe the initial spectral dependence function  
60 used by the Auger Observatory in section 2. The new light source used in  
61 the procedure is described in section 3 and its characterisation in section 4.  
62 The FD-telescope wavelength response and a discussion of uncertainties are  
63 presented in section 5.

## 64 2. Piecewise spectral response of the fluorescence detector

65 The spectral response of the FD originally used by the Auger Observatory  
66 was assembled from the efficiencies of the individual telescope components.  
67 The individual efficiencies were obtained from statements by the component  
68 manufacturers or, in some cases, as measured by members of the Pierre  
69 Auger Collaboration [9]. The elements considered for the spectral response  
70 were the UV filter and corrector ring transmission, the mirror reflectivity, and  
71 the PMT quantum efficiency. The overall wavelength response is dominated  
72 by filter and PMT effects. We call this piece-wise curve  $PW(\lambda)$  and show it  
73 in section 5 to compare it with results in Fig. 7.

74 Regardless of the accuracy of the measurements on each telescope com-  
75 ponent, the fact that the response of the system was not measured as a whole  
76 indeed introduces uncertainties. We can calculate, for example, that the cor-  
77 rector ring transmission does not affect all the incoming photons but only  
78 approximately half of them, when camera shadowing effects are included.  
79 Also, the reflectivity of the light concentrators in the camera are not taken  
80 into account at all, even though a third of the light getting to the pixel is  
81 reflected by them. There are other less important considerations such as  
82 the fact that mirrors for the FD telescopes are made using two different  
83 techniques by two different manufacturers [10]. One of them is a machined  
84 aluminium alloy with a protecting layer of  $\text{Al}_2\text{O}_3$  at its reflecting surface. In  
85 the second technique polished glass is aluminized and the reflecting surface  
86 is covered by a layer of  $\text{SiO}_2$ . Both types of mirrors have similar reflectivities  
87 as measured at 370 nm [10]. However, considering that they use different di-  
88 electric coatings on different materials, the reflectivity at other wavelengths  
89 may vary.

90 To assure that the Pierre Auger Observatory is using the right spectral  
91 response of its FD telescopes, the decision was made to adapt the end-to-end  
92 procedure used for absolute calibration to directly measure this function.

### 93 3. Multi-wavelength light source

94 To enable multiple wavelength measurements, the LED used for absolute  
95 calibration was removed and a light pipe was installed between the Teflon  
96 diffuser and the back of the drum, where new light sources could be mounted  
97 (see Fig. 2). A xenon flasher is mounted at the end of the pipe at the  
98 back of the drum. The xenon flasher<sup>2</sup> provides 0.4 mJ optical output per  
99 pulse covering a broad UV spectrum, in a time period of a few hundred  
100 nanoseconds. To select a desired wavelength, notch-filters<sup>3</sup> are mounted in  
101 a filter wheel attached to the end of the pipe. A focusing lens at the filter  
102 wheel output maximises the intensity through the filter wheel and into the  
103 light pipe. Notch-filters were chosen at five wavelengths inside the range  
104 of the FD UV filter located at the telescope aperture. According to the  
105 manufacturer, the filter transmissions are centred at 320, 337, 355, 380 and  
106 405 nm, with a FWHM  $\approx$  15 nm.

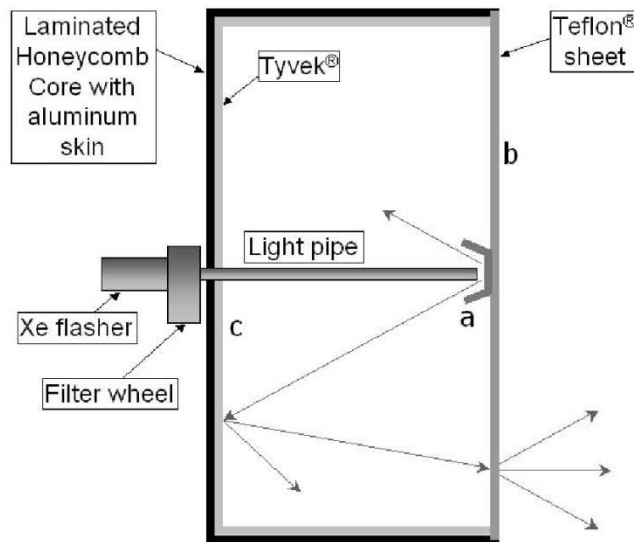


Figure 2: Drum section showing the main components of the light source. The diffusively reflecting surfaces a) and b) are Teflon, while c) is Tyvek

<sup>2</sup>RSL-2100 series xenon flasher - Perkin Elmer, [www.perkinelmer.com](http://www.perkinelmer.com)

<sup>3</sup>Standard UV bandpass filters, Andover Corporation, [www.andcorp.com](http://www.andcorp.com)

## 107 4. Characterization Measurements

108 The drum relative intensity is measured at each wavelength in a dedicated  
109 calibration laboratory at the Observatory. An auxiliary PMT, the “lab-PMT”,  
110 is used to measure the light intensity of the drum for a given notch-filter.  
111 Quantum efficiency (QE) of the lab-PMT and FD spectral response have  
112 significant variations within the range of wavelengths where the notch-filters  
113 transmit. To understand the corrections to be applied due to these variations  
114 we have performed measurements described in the following sections.

### 115 4.1. Notch-filter transmission scan

116 Notch-filters listed in section 3 were selected at 5 wavelengths either near  
117 the main emission bands of nitrogen [11] used for EAS fluorescence detection  
118 (320, 355 and 405 nm), or to match the laser wavelengths (337 and 355 nm)  
119 used in previous absolute calibration cross checks using roving lasers [5], or  
120 near the 375 nm LED single-wavelength absolute calibration. Precise mea-  
121 surements of the transmission characteristics of each notch-filter are needed.  
122 The filters were scanned using a monochromator with a broadband deuterium  
123 light source. A photo-diode of known wavelength dependence [12] was used  
124 at the monochromator output to detect the transmitted light as a function of  
125 wavelength in 2 nm steps. The results are shown in Fig. 3 where the spectral  
126 shape of the deuterium light source and the response of the photo-diode have  
127 been deconvolved. We assign labels of  $f_i(\lambda)$  to the curves in the figure and  $\lambda_i$   
128 to the central wavelength of each of them, where  $i = 1, 5$  indicates one of the  
129 five notch-filters (from 320 nm to 405 nm). A scan from the manufacturer  
130 was available for one of the filters (337 nm), and it was found to be in good  
131 agreement with our scan. Some asymmetries were found in the transmission  
132 curves (320 and 337 nm) that make significant differences when applying  
133 filter corrections.

### 134 4.2. Quantum efficiency of the lab-PMT

135 We measured the relative quantum efficiency of the lab-PMT in 2 nm  
136 steps using the deuterium light source and the monochromator. We directed  
137 the monochromator output through a thin Teflon diffusor and into a dark  
138 box containing the lab-PMT and a NIST-calibrated photo-diode<sup>4</sup> [12]. Using  
139 the small photo-diode we verified that the beam was uniform laterally at a

---

<sup>4</sup>UV100 photodiode, UDT Sensors, Inc, Hawthorne, CA USA

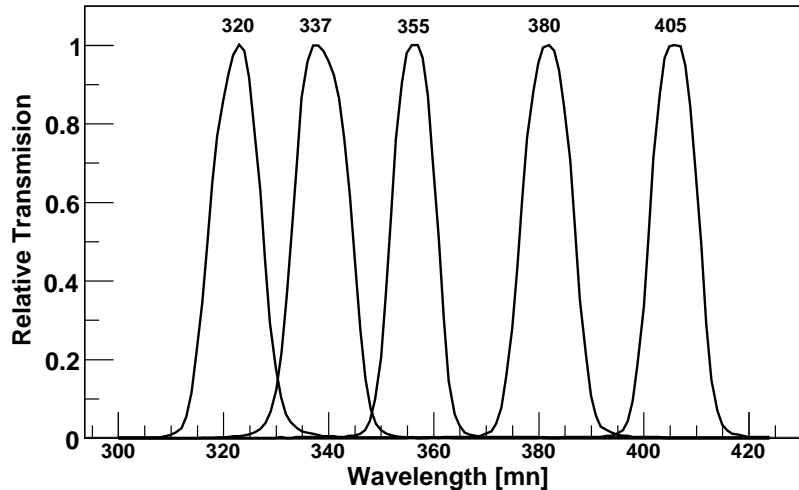


Figure 3: Relative transmission of the notch-filters used for multi-wavelength calibration. The nominal wavelength is indicated for each filter

140 level of 0.5% over an area larger than the PMT photochathode. The first  
 141 step in the QE measurement was to scan the monochromator and measure  
 142 the relative output intensity in photons at each wavelength, using the photo-  
 143 diode and it's known calibration. Then, using an iris to limit the intensity  
 144 and prevent PMT saturation, we rescanned the source and measured the  
 145 PMT current. The PMT relative QE as a function of wavelength,  $QE(\lambda)$ , is  
 146 the ratio of these two scan results at each wavelength.

147 The measured QE, shown in Fig. 4, is in agreement with the average  
 148 photocathode QE provided by the manufacturer<sup>5</sup>, within the measurement  
 149 uncertainties of 2.5%, which are discussed in section 5.2.

#### 150 4.3. Drum Intensity at five wavelengths

151 With the notch-filter wheel mounted on the drum, the relative intensity of  
 152 the drum surface for each wheel position depends on the xenon source inten-  
 153 sity at the transmitted wavelengths, the notch-filter transmission and losses  
 154 in the light pipe. No wavelength shifting of photons of Teflon and Tyvek

---

<sup>5</sup>78 mm, 9265B PMT, made by Electron Tubes, [www.electrontubes.com](http://www.electrontubes.com)

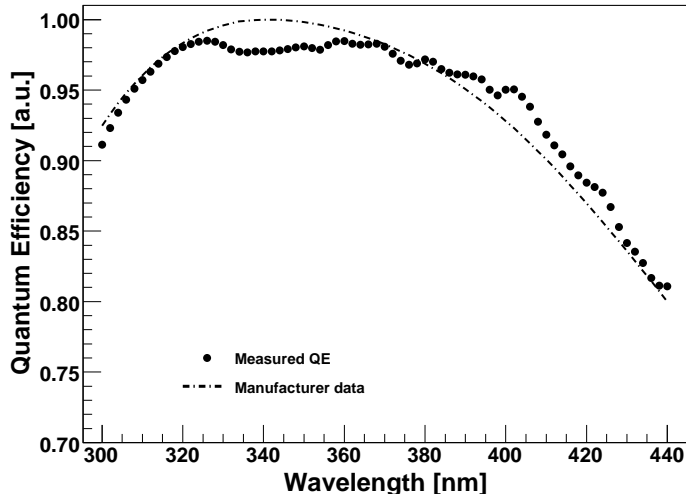


Figure 4: The measured quantum efficiency of the lab-PMT used in this work, and the typical QE from the manufacturer’s specification sheet

155 materials has been observed in our independent laboratory measurements.  
 156 Ideally, to measure the drum intensity for each wavelength, one would use  
 157 the drum surface as input to the monochromator and scan the full spectrum  
 158 for each notch-filter. In practice this is precluded by the low drum intensity.  
 159 Instead, we make a single measurement of the integrated drum intensity for  
 160 each notch-filter using the lab-PMT. For each notch-filter we find a value  
 161 for  $C_i$ , the centroid of the histogram of the PMT response to 1000 xenon  
 162 flasher pulses. These centroids are proportional to the drum intensity for  
 163 each notch-filter once corrections have been made for variations in lab-PMT  
 164 QE. Ignoring common constants,  $\int \Phi_i(\lambda) QE(\lambda) d\lambda = C_i$ , where  $\Phi_i(\lambda)$  is  
 165 the brightness of the drum surface for the notch-filter  $i$  as a function of  
 166 wavelength. Then, since the distribution of drum photons is the convolution  
 167 of the known xenon flasher spectrum,  $Xe(\lambda)$ , and the corresponding notch-  
 168 filter, we use  $\Phi_i(\lambda) = k_i f_i(\lambda) Xe(\lambda)$  and adjust  $k_i$  to match the integral  
 169 above. With this last process all five values of drum brightness and their  
 170 wavelength distributions are known.

171 The quantity  $\int \Phi_i(\lambda) d\lambda = \Phi_i$  is proportional to the real total photon flux  
 172 being emitted by the drum surface. All the wavelength independent prop-  
 173 erties (PMT gain, electronic conversion, etc.) are left out because they will

174 cancel in the end when the relative values are computed. We also note that  
 175  $\Phi_i$  is not significantly different from the value it would have if the function  
 176  $QE(\lambda)$  was totally flat within the notch-filter range. Then, in practice,

$$\int \Phi_i(\lambda) d\lambda = \Phi_i \simeq C_i/QE(\lambda_i) \quad (1)$$

## 177 5. Fluorescence Detector response to drum

178 For testing the procedure we use results of measurements made at one  
 179 FD telescope. In August 2006 we mounted the drum with xenon flasher and  
 180 filter wheel at the aperture of telescope 4 at the Los Leones FD-building. A  
 181 series of 400 xenon flashes illuminated the camera, and we found the average  
 182 integrated pulse for each pixel. In Fig. 5 we show the response of one FD  
 183 pixel and the distribution of pulse integrals for the same pixel. The pulse  
 184 shape from the drum with the xenon source is irregular and varies from pulse  
 185 to pulse, but the total output energy is consistent as indicated by the <10 %  
 186 RMS of the integral distributions. We obtained the average charge from the  
 187 distributions of those 400 pulse integrals,  $I_{i,j}$ , for each notch-filter  $i$  and each  
 188 pixel  $j$ . Typical statistical uncertainty for these values is <0.5 %.

189 The relative wavelength-dependent FD response for pixel  $j$  is then the  
 190 ratio of the integrated ADC response of the FD to the relative number of  
 191 photons at the aperture. We call this value  $R_{i,j}$  so that  $R_{i,j} = I_{i,j}/\Phi_i$ . A  
 192 considerable dispersion of  $R_{i,j}$  values is expected as pixels have different gains  
 193 and amplifications. However, we are only interested in relative wavelength  
 194 responses so, all values are normalized to the response to the 380 nm notch-  
 195 filter, or  $i = 4$ . Thus  $R_{i,j}^{rel} = R_{i,j}/R_{4,j}$ . In Fig. 6 the distribution of these  
 196 relative responses for pixels in the measured telescope is shown for each notch-  
 197 filter, except the one at 380 nm as this would be the identity. The histograms  
 198 shown for each notch-filter in Fig. 6 have relatively low dispersions, ranging  
 199 from 1.1% to 2.2% RMS. We consider that the relative response for each  
 200 PMT in the camera is well represented by the average of those distributions,  
 201 so only one value for each notch-filter is taken. We call these values  $R_i^{rel}$ ,  
 202 where  $i$  identifies the filter.

203 In Table 1 we show the  $R_i^{rel}$  values obtained for the telescope as evaluated  
 204 from the distributions on Fig. 6. Uncertainties to these values are discussed  
 205 in next sections. The resulting wavelength dependent efficiency is shown in  
 206 Fig. 7 where the fitting was done adjusting the piecewise function to the

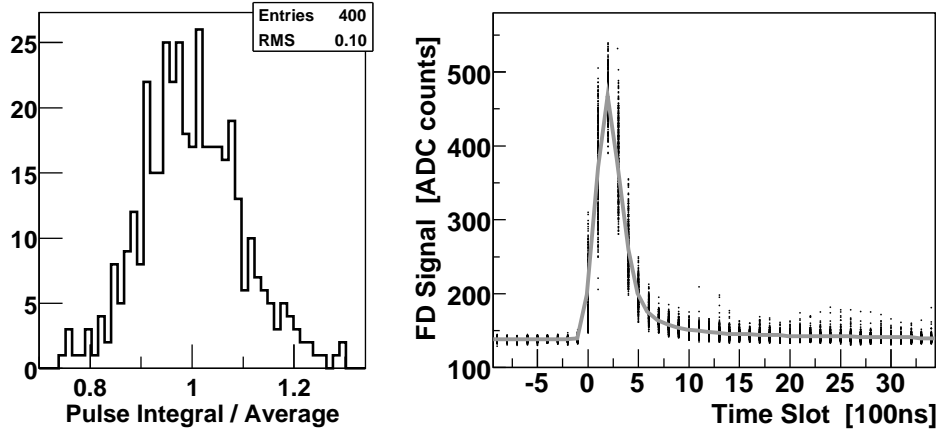


Figure 5: FD single pixel response to drum pulses. The signal of pixel number 220 of telescope 4 with drum at 355 nm is shown. Left: Distribution of pulse integrals related to the average integral. Right: Pulses as registered by the FD. Dots are the values for 400 individual pulses. The grey solid line is the average

207 five measured points  $R_i^{rel}$ . The piecewise response in its original form is also  
 208 shown in the figure for comparison purposes. The fit has been corrected for  
 209 notch-filter width effects, as described in next section.

#### 210 5.1. Notch Filter Width Effects and fitting procedure

211 In section 4.3 we described how the drum centroids for five wavelengths  
 212 were measured and corrected for the lab-PMT quantum efficiency to get the  
 213 relative drum intensities. In that process the change in the QE was taken  
 214 into account by considering the distribution of photons for each notch-filter.  
 215 Then, in section 5, we described how the FD responses to those intensities  
 216 were measured for one FD telescope. In this last process the notch-filter  
 217 width effect was not taken into account. Because the overall FD response is  
 218 not flat in the  $\sim 15$  nm FWHM range of each filter, this uncorrected result is  
 219 biased toward the region of the filter corresponding to higher FD response.

220 To correct for this effect we follow a similar procedure as in section 4.3.  
 221 The process at the telescope is:

$$\frac{\int \Phi_i(\lambda) FD(\lambda) d\lambda}{\int \Phi_i(\lambda) d\lambda} = R_i^{rel} \quad (2)$$

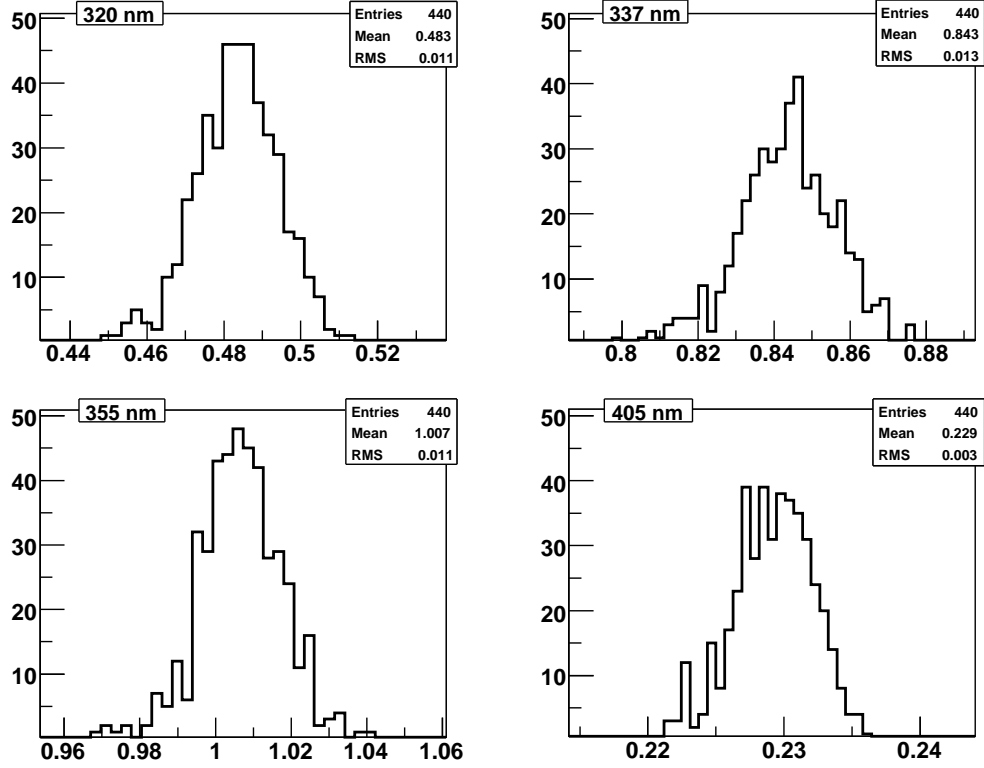


Figure 6: Distribution of relative FD response for each notch-filter. The response relative to 380 nm of all pixels in one telescope is shown

222 where  $FD(\lambda)$  is the FD relative response as a function of wavelength.  
 223 Again, we are not including wavelength independent constants as this is a  
 224 relative measurement procedure. Note that if the notch-filter transmission,  
 225  $f_i(\lambda)$ , were delta functions at  $\lambda_i$ , we would have  $FD(\lambda_i) = R_i^{rel}$ . To solve the  
 226 integral of equation 2 and find the unknown function  $FD(\lambda)$  we made the  
 227 assumption that the FD response is a piecewise-like function, as described  
 228 in section 2. This choice is required because the five measurements in the  
 229 wavelength range of the FD response are not sufficient to fully characterise  
 230 a generic function. Then, it is reasonable to adjust the original piecewise  
 231 function,  $PW(\lambda)$ , to what was measured. This assumption also implies that  
 232 we have taken the FD response as null beyond the wavelength of the FD

Wavelength (nm)	$R_i^{rel}$	
	Mean	Corrected
320	0.483	0.409
337	0.843	0.832
355	1.007	0.998
380	1.000	1.044
405	0.229	0.243

Table 1: Average relative FD response measured for each notch-filter. Values are taken from the distributions of Fig. 6. The column on the right have the values after the correction for notch-filter width effects as described in section 5.1

233 system. Particularly, we take  $FD(280\text{ nm}) = FD(425\text{ nm}) = 0$ , which have  
 234 been verified by measuring the UV-filter transmission in our laboratory.

235 The procedure of adjusting the fitting function to the measured points was  
 236 as follows. For each notch-filter we take  $FD(\lambda) = h_i Fit(\lambda)$ , where  $Fit(\lambda)$   
 237 is the fitting function and  $h_i$  a parameter for filter  $i$ . As a first guess the  
 238 piecewise function is taken so,  $Fit(\lambda) = PW(\lambda)$ . Equation 2 is evaluated and  
 239 the parameter  $h_i$  found to match the value  $R_i^{rel}$ . Once all five  $h_i$  are found,  
 240 a new fit is done by interpolating the points  $h_i Fit(\lambda_i)$  with a piecewise-like  
 241 function, where now  $i$  runs for seven points, including the null extremes.  
 242 Between these points, the curve is adjusted by a linear interpolation of the  
 243 adjustments at the surrounding points. Finally, this last fit is taken as a new  
 244  $Fit(\lambda)$  function and the process starts again until all five values  $h_i$  are the  
 245 identity.

246 The final result of the iteration procedure,  $Fit(\lambda)$ , is the  $FD(\lambda)$  that  
 247 fulfils the integral in equation 2 for all five measured points. This curve is  
 248 shown in Fig. 7, normalised to the value at 380 nm. In the same figure we  
 249 also show the original piecewise function. A decrease in the spectral response  
 250 compared to the piecewise response is observed at shorter wavelengths, the  
 251 largest difference of  $\approx -28\%$  comes at 320 nm. The corrected  $R_i^{rel}$  values are  
 252 shown in Table 1.

## 253 5.2. Uncertainties

254 Contributions to the uncertainty include those from measurements in the  
 255 laboratory of the drum intensity, and from measurements at the telescope  
 256 of the FD response. The overall result reported here is a relative measure-  
 257 ment, and consequently many factors cancel particularly systematics related

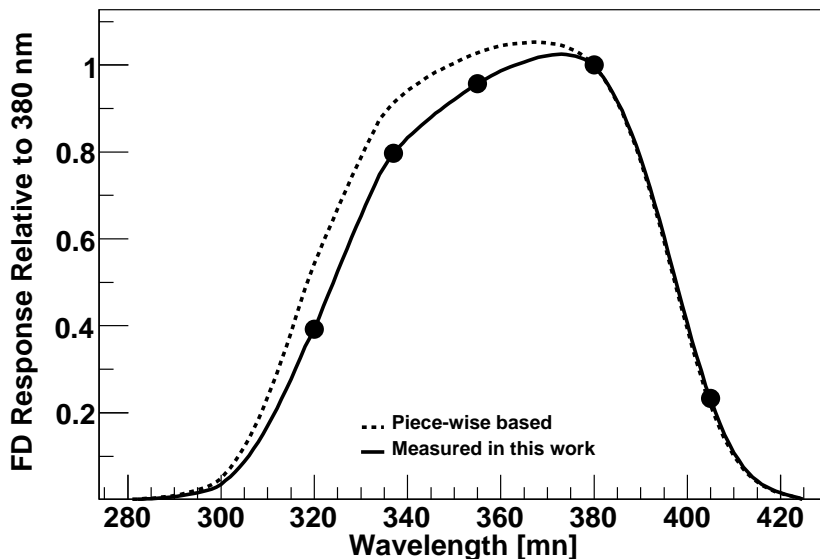


Figure 7: The measured Fluorescence Detector wavelength response compared with a curve generated in a piecewise fashion from manufacturer’s data for each FD component. The corrected measurements at the 5 wavelengths are shown; the solid curve is constrained to pass through those points

258 to laboratory setup.

259

260 The determination of drum intensity at each wavelength includes mea-  
 261 surements in the laboratory of the centroid of the lab-PMT response to pulsed  
 262 drum illumination, and the relative QE of the lab-PMT. The uncertainty in  
 263 the lab-PMT drum response centroid,  $C_i$  in equation 1, is estimated to be 1  
 264 channel in the ADC converter plus the statistical uncertainty on the mean  
 265 of the 1000 xenon pulse distribution. The 1 channel uncertainty is a system-  
 266 atic effect, related to repeatability, and has more relevance for wavelengths  
 267 where the drum brightness is low. The second column in Table 2 indicates  
 268 the uncertainties in  $C_i$ .

269 Uncertainties related to measurement of the relative QE of the lab-PMT  
 270 include those from lab-PMT response, photodiode current during monochro-  
 271 mator scans, the calibration of the photodiode at each wavelength, and sys-  
 272 tematics in the laboratory setup. The uncertainty in the monochromator

Wavelength (nm)	$C_i$ (%)	$\Phi_i$ (%)	$R_i^{rel}$ (%)		
			Statistical	Systematic	Total
320	0.6	2.6	2.2	4.1	4.7
337	1.0	2.7	1.5	4.2	4.5
355	2.0	3.2	1.1	4.5	4.6
380	2.0	3.2	n/a	0.0	0.0
405	0.3	2.5	1.3	4.1	4.3

Table 2: Sources of uncertainties and their values for this work (see section 5.2).

273 wavelength has been measured with a N2 laser light source to be less than  
274  $\sim 0.25$  nm, and no contribution to the overall uncertainty has been included  
275 for this effect.

276 For the PMT QE scans, currents from the photodiode and the lab-PMT  
277 were measured with electronics based on an integration chip with linearity  
278 of 0.005% [13]. Effects of connectors and cabling between the detectors and  
279 the integration chips are expected to dominate any nonlinearities. While  
280 these effects are expected to be small, we assign an overall uncertainty of 2%  
281 to current measurements, based on our experience measuring absolute cur-  
282 rents using similar configurations. For this relative measurement, the exper-  
283 imental configuration remained unchanged during measurements at different  
284 wavelengths, allowing some readout systematics to cancel in the final ratios.  
285 The uncertainties in the absolute response of the photodiode, as calibrated  
286 by NIST, are documented as k=2 expanded uncertainties [12]. Assuming  
287 normal distributions for the contributing factors, these can be interpreted  
288 as 1-sigma uncertainties varying in the range from 0.55 to 0.95% for wave-  
289 lengths between 300 and 400 nm, and 0.4% or less for those between 405 and  
290 450 nm. Monochromator output beam uniformity has been measured in the  
291 PMT-photodiode region to be better than 0.5% across a 10 cm region per-  
292 pendicular to the beam. No contribution to the overall uncertainty has been  
293 included for beam non-uniformity. The stability of the system, including the  
294 lab-PMT response, was tested by performing measurements multiple times  
295 to find that repeatability is well within 1%. As a result of these effects we  
296 consider an overall uncertainty of 2.5% for the relative QE of the lab-PMT.  
297 Combination of the uncertainties of  $C_i$  and QE give the uncertainty in the  
298 drum brightness,  $\Phi_i$ , as listed in Table 2.  
299

300 The camera-averaged response of pixels to each of the five wavelengths  
 301 are described in section 5. To evaluate the uncertainties in these responses  
 302 we consider the systematics coming from drum fluxes,  $\Phi_i$  as discussed above,  
 303 and the widths of the distributions of responses for the 440 pixels in the  
 304 camera, as taken from the distributions of Figure 6 and shown in the fourth  
 305 column of Table 2. For a given pixel  $j$ ,  $R_{ij}^{rel} = R_{ij}/R_{4j}$ , four quantities have  
 306 to be considered: two integrals,  $I_{ij}$  and  $I_{4j}$ , and two drum fluxes,  $\Phi_i$  and  
 307  $\Phi_4$ , as defined in previous sections. Uncertainties in the integrals are purely  
 308 statistical and have been evaluated to be  $<0.5\%$ . The combination of these  
 309 four values gives the total uncertainty shown in the fifth column of Table 2.  
 310 Values at different wavelengths are independent and are added in quadrature,  
 311 except at 380 nm where systematic uncertainties are null by definition. The  
 312 last column in Table 2 shows the combined uncertainty for the two sources.  
 313

314 Finally, we consider uncertainties resulting from the fitting procedure  
 315 incorporating the effects of the notch-filter widths, as described in section  
 316 5.1. The shape of the piecewise calibration curve, used as the initial fitting  
 317 function, is dominated near 300 nm by the fall-off of FD PMT quantum  
 318 efficiency at shorter wavelengths, and by decreasing transmission of the UV  
 319 filter through the FD aperture above 400 nm. We have tried several shapes  
 320 for this initial function and found that any reasonable choice incorporating  
 321 these two features leads to near-identical results. No related uncertainty is  
 322 included.

323 When applying the notch-filter width correction we use the relative trans-  
 324 mission of the 5 notch filters, measured as described in section 4.1. Associ-  
 325 ated uncertainties are  $0.5\%$  at each wavelength in the scans. Good correlation  
 326 with the manufacturer's scan available for one filter supports this value of  
 327 the uncertainty. For an independent evaluation of the systematics related  
 328 to filter shape, we took the wavelength with the largest filter-width effect,  
 329 320 nm, and changed the filter shape to an extreme-case scenario of a step  
 330 function. We included a maximum spread in intensity between two wave-  
 331 lengths by assuming extremes of the photodiode uncertainties at the respec-  
 332 tive wavelengths. We then repeated the notch filter correction calculation.  
 333 The corrected value of  $R_1^{rel}$  given in Table 1 changed by  $-0.5\%$ , supporting  
 334 the assesment above.

335 Based on the discussions above, we assign an overall total uncertainty  
 336 of  $5\%$  to the measurements reported here. The main contributions come  
 337 from the uncertainties on the relative QE of the lab-PMT and the measured

338 relative drum fluxes at each wavelength.

## 339 **6. Conclusions**

340 The method for measuring the relative wavelength-dependence response  
341 of the Pierre Auger fluorescence detector has been tested in one telescope.  
342 Within uncertainties we can say that a multi-wavelength calibration for each  
343 PMT in a given camera is not necessary as the dispersion around the average  
344 is of the order of few percent.

345 This result indicates lower FD efficiency at shorter wavelengths when  
346 compared to a curve constructed in a piecewise manner from manufacturer  
347 efficiency specifications for the individual elements of the system. The piece-  
348 wise curve was adjusted to the measured values and the result is currently  
349 used in the Auger event reconstruction software.

## 350 **References**

- 351 [1] J. Abraham [Pierre Auger Collaboration], NIM A 523 (2004) 50-95.
- 352 [2] M. Roth [Pierre Auger Collaboration], Proceeding 30<sup>th</sup> ICRC, Merida  
353 (2007).
- 354 [3] J. Abraham [Pierre Auger Collaboration], Physical Review Letters 101  
355 (2008), 061101.
- 356 [4] V. Verzi [Pierre Auger Collaboration], Nucl. Phys. B (Proc. Suppl.) 165  
357 (2007) 37.
- 358 [5] R. Knapik [Pierre Auger Collaboration], Proceeding 30<sup>th</sup> ICRC, Merida  
359 (2007).
- 360 [6] C. Aramo [Pierre Auger Collaboration], Proceeding 29<sup>th</sup> ICRC, Pune  
361 (2005), 8, 101.
- 362 [7] J. T. Brack, *et al.*, Astropart. Phys. 20 (2004) 653.
- 363 [8] P. Bauleo [Pierre Auger Collaboration], Proceeding 29<sup>th</sup> ICRC, Pune  
364 (2005), 8, 5-8.

- 365 [9] J. A. J. Matthews [Pierre Auger Collaboration], Proceeding SPIE As-  
366 tronomical Telescopes and Instrumentation, Waikoloa , Hawaii (2003),  
367 4858, 121-130.
- 368 [10] G. Matthiae [Pierre Auger Collaboration], Proceeding 27<sup>th</sup> ICRC, Ham-  
369 burg (2001).
- 370 [11] M. Nagano, *et al.*, Astropart.Phys. 20 (2003) 293.
- 371 [12] T.C. Larson, S.S. Bruce, and A.C. Parr, “Spectroradiometric Detector  
372 Measurements”, National Institute of Standards and Technology, Cal-  
373 ibration Program, Gaithersburg, MD 20899-2330, Special Publication  
374 250-41, 1998.
- 375 [13] Burr-Brown Corporation, chip ivc102; <http://www.burr-brown.com/>